Pathways for the Formation of C_{2+} Products Under Alkaline Conditions during the Electrochemical Reduction of CO_2

Joseph A. Gauthier,[†,‡,¶] Zhou Lin,[†,§,‖] Martin Head-Gordon,[*,†,§] and Alexis T. Bell[*,†,‡]

†*Chemical Sciences Division, Lawrence Berkeley National Laboratory, Berkeley, California 94720, USA*

‡*Department of Chemical and Biomolecular Engineering, University of California, Berkeley, California 94720, USA*

¶*Department of Chemical Engineering, Texas Tech University, Lubbock, TX 79409*

§*Kenneth S. Pitzer Center for Theoretical Chemistry, Department of Chemistry, University of California, Berkeley, California 94720, USA*

‖*Department of Chemistry, University of Massachusetts Amherst, Amherst, MA 01003*

E-mail: mhg@cchem.berkeley.edu; alexbell@berkeley.edu

Abstract

Establishing how Cu facilitates the electrochemical CO_2 reduction reaction (CO2RR) to products with more than one carbon atom, C_{2+}, remains a critical challenge towards achieving economic viability of the process. Under typical reaction conditions, both the bulk pH and local pH are alkaline, with the pH near the electrode being considerably more alkaline due to poor transport of hydroxide anions. Challenges with probing alkaline pathways using computational methods has limited understanding of the CO2RR

under experimentally relevant conditions. In this work, we demonstrate that predicted activation barriers can substantially differ between the acidic and alkaline pathway, using the Volmer reaction on Cu (100) as a test case. We compute reaction energetics for alkaline ∗CO protonation and find that while the formation of ∗CHO is preferred thermodynamically, formation of ∗COH is more favorable kinetically at high overpotential. We find, however, that the formation of ∗CHO by the reaction of adsorbed ∗H and ∗CO is feasible at room temperature. We report potential dependent energetics for forming the first C-C bond in CO_2 reduction, and find that this process is likely driven by CO dimerization. Finally, we investigate how inclusion of long-range van der Waals interactions impacts the predicted results by comparing to the meta-GGA B97M–rV.

Consumption of fossil fuels and the corresponding release of CO_2 has lead to an imbalance in the global carbon cycle, resulting in significant changes to the global climate.[1] This concern has stimulated interest in the electrochemical CO_2 reduction reaction (CO2RR) as a means to transform CO_2 into useful fuels and feedstock chemicals. Since the CO2RR is unfavorable both thermodynamically and kinetically, a source of energy and an appropriate catalyst are required.[2] To date, Cu is the only known electrocatalyst that leads to the formation of economically attractive products with more than one carbon (C_{2+}), with all other known catalysts producing only H_2(g) and single carbon (C_1) products.[3] The detailed mechanisms for the synthesis of C_{2+} products on Cu are therefore of great interest, in particular the structures and energetics of intermediate species that dictate the selectivity and activity of the catalyst.

While experimental approaches to studying electrocatalysis have advanced considerably in the past decade, probing intermediate species *in-operando* remains a challenge.[4] Computational approaches to modeling the electrochemical interface have emerged to fill this void and provide a reasonable pathway to identifying critical intermediate species and mechanisms for a variety of reaction chemistries.[5] Investigating the alkaline pathway of the CO2RR, in which water is the proton source and produces hydroxide ions, has known challenges for computa-

tional studies, particularly those relying on an explicit electrolyte representation.[6–8] Nearly all computational studies of the CO2RR to date have therefore investigated the acidic pathway, where the proton source is hydronium cations.[9–16] However, recent experiments suggest that even in the case of the bulk electrolyte pH being highly acidic, the pH near the interface is alkaline at operating conditions due to hydroxide anion transport limitations.[17–19] Furthermore, most experiments are conducted with neutral to alkaline bulk pH, resulting in an even higher local pH near the interface and limiting the availability of hydronium cations at an active site.[18–27] Considering the importance of the electrolyte pH on electrocatalysis[28–34] and the likely absence of hydronium cations near the interface *in-operando*, in this work we investigate the alkaline pathway for the formation of C_{2+} products during the CO2RR.

To demonstrate the importance of considering the alkaline pathway when investigating electrocatalytic mechanisms, we computed reaction energies and activation barriers for the Volmer reaction on Cu (100), with both water and hydronium cations as the proton source. The alkaline and acidic Volmer reactions are given in Equations 1 and 2 respectively,

$$* + H_2O + e^- \rightarrow *H + OH^- \tag{1}$$

$$(H^+ + e^-) + * \rightarrow *H \quad . \tag{2}$$

We utilized an implicit electrolyte (VASPsol) with constant potential methodology[35–39] (see supplementary information (SI) Notes 1 and 2), and two water molecules to assist in solvation of the hydronium cations or hydroxide. We find this to reasonably reproduce experimental solvation energies (see SI Note 3). Additionally, the correction of Chan and coworkers[7,31,40,41] which leverages the computational hydrogen electrode (CHE)[42] and corrects for the incomplete solvation and partial hybridization[43] of the hydronium cations near the surface, was adapted to correct for hydroxide near the surface. In the case of the acidic pathway, this correction affects both the reaction energy and activation barrier, as the initial state is the state adjusted. In the case of the alkaline pathway, only the reaction energy is affected,

while the (forward) barrier is not, since the final state is adjusted. Further details of this correction can be found in SI Note 4. The computed energetics are shown in Figure 1(A).

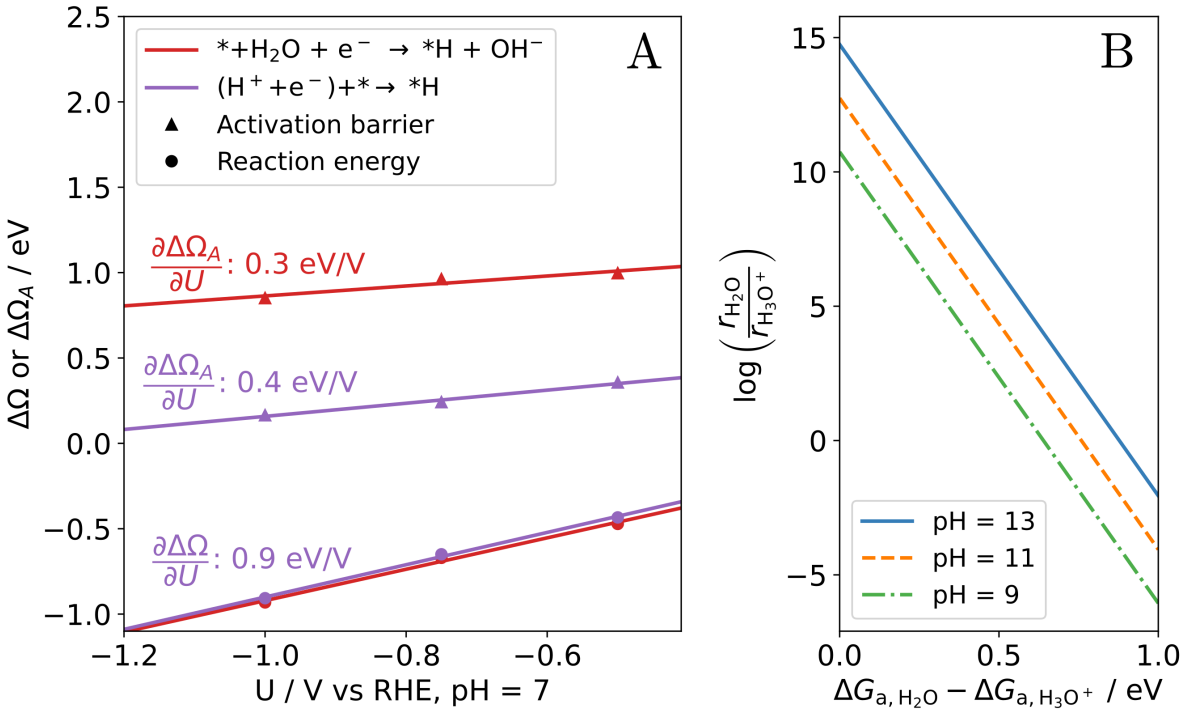

Figure 1: (A) Calculated reaction energies and activation barriers for the Volmer reaction on Cu (100). Red points represent the alkaline pathway, while purple represents the acidic pathway. While no difference is found for the reaction energy, the activation barrier in the alkaline pathway is about 0.7 eV higher, with a similar transfer coefficient. Transition states were identified using a sequence of constrained bond–length geometry optimizations to overcome convergence problems with the dimer method. Where possible, results were benchmarked to the dimer method,[44] with a charge neutral climbing image nudged elastic band[45,46] providing the initial guess. See SI Note 1 for further details. (B) Relative rates of the alkaline and acidic pathways for a generic coupled proton electron transfer as a function of the barrier difference and the local pH.

Due to the aforementioned correction to the initial state of the acidic pathway and to the final state of the alkaline pathway (SI Note 4), we correctly find the reaction energy does not depend on the pathway chosen. However, we find a substantial difference in the computed activation barriers when comparing the alkaline and acidic pathways of the Volmer reaction on Cu (100). Our result mirrors a theoretical study of hydrogen evolution on Pt (111) by Chan and coworkers[31] and is supported experimentally by Markovic and coworkers,[30]

who found substantially later onset of hydrogen evolution in alkaline conditions. This later onset can be easily ascribed to insufficient concentration of hydronium cations to support the acidic pathway in alkaline conditions. Instead, activity is driven largely by the alkaline pathway; the substantially higher activation barrier found for this pathway therefore leads to a later onset. While we do not attempt to fully reproduce all activation barriers along the HER pathway in acidic and alkaline media as was done by Chan and coworkers, our results highlight the need to consider the alkaline pathway for CPET reactions when the bulk pH is neutral to alkaline as is typically the case in the CO2RR. Indeed, several experimental and theoretical investigations have identified a substantial increase in the electrolyte pH near the surface relative to bulk due to limiting transport of hydroxide anions,[18–27] further inhibiting the acidic pathway. The effect of the decreased local hydronium cations concentration on the reaction energetics can be approximated by assuming an Eyring-like expression for the rate-limiting CPET step:

$$r_{\mathrm{H_3O^+}} = \frac{k_B T}{h} c_{\mathrm{H_3O^+}} \exp\left[-\frac{\Delta G_{\mathrm{a,H_3O^+}}}{k_B T}\right] \tag{3}$$

$$r_{\mathrm{H_2O}} = \frac{k_B T}{h} c_{\mathrm{H_2O}} \exp\left[-\frac{\Delta G_{\mathrm{a,H_2O}}}{k_B T}\right] \quad . \tag{4}$$

Here, r_i refers to the rate of either the acidic or alkaline pathway, k_B the Boltzmann constant, T the temperature, h Planck's constant, c_i the activity of either hydronium cations or water, and ΔG_a the activation barrier of the acidic or alkaline pathway (as computed in panel A of Figure 1). We can approximate the activity of hydronium cations as the local concentration of hydronium cations, i.e. $c_{\mathrm{H_3O^+}} = 10^{-\mathrm{pH}}$, and take the activity of water to be 55.5M. The orders of magnitude difference in activity lends itself to a significant effective barrier. By dividing these two rate equations, we can see that the relative rate of the alkaline and acidic pathways depend on the relative concentration of water and hydronium cations,

$$\frac{r_{\mathrm{H_2O}}}{r_{\mathrm{H_3O^+}}} = \left(\frac{c_{\mathrm{H_2O}}}{c_{\mathrm{H_3O^+}}}\right) \exp\left[-\frac{\Delta G_{\mathrm{a,H_2O}} - \Delta G_{\mathrm{a,H_3O^+}}}{k_B T}\right] \tag{5}$$

The result of this calculation is plotted in panel B Figure 1. We estimate a significant contribution from the alkaline pathway at high local pH though the alkaline barrier is significantly higher. Based on our analysis and our calculations below, we suggest that the alkaline pathway is at least competitive with, and sometimes faster than, the acidic pathway, despite the higher forward activation barrier.

For reaction chemistries such as the HER, where current is largely driven by coupled proton electron transfers (the Tafel reaction is thought to be negligible at reasonably high overpotentials[41]), the existence of a linear scaling between the acidic and alkaline activation barriers would result in activity trends for the acidic pathway that match trends for the alkaline pathway. Such a scaling would allow for theoretical investigations to rely only on the simpler to compute acidic pathway, with the results being directly extendable to the alkaline pathway. However, to our knowledge, no such scaling has been demonstrated. Furthermore, for reaction chemistries such as the CO2RR, where activity is driven by a combination of CPET steps (e.g., protonation of adsorbed CO) and chemical steps (e.g., C-C bond formation), the existence of such a scaling would not allow for reliance on the acidic pathway for CPET steps. Given the likelihood of poor availability of hydronium cations at the cathode surface even when the bulk pH is acidic, substantial differences in computed activation barriers between the alkaline and acidic pathway, and the competition between CPET and chemical steps in the CO2RR, we suggest that the alkaline pathway is more likely to be physically relevant in the CO2RR.

Bearing in mind that the alkaline pathway is more physically relevant, we computed the reaction energy and activation barriers associated with CO protonation on Cu (100) with water as the proton source. We use the same approach as with the Volmer reaction, i.e. a constant potential approach with implicit electrolyte[38,39] in addition to three explicit waters in the initial state, and two water molecules and a hydroxide in the final state. As before, transition states were identified using a sequence of contrained bond–length geometry optimizations benchmarked to the dimer method,[44] with further details being provided in SI

Note 1. We again correct the final state for incomplete solvation of the hydroxide and partial hybridization with the surface. The computed reaction energetics are shown in Figure 2.

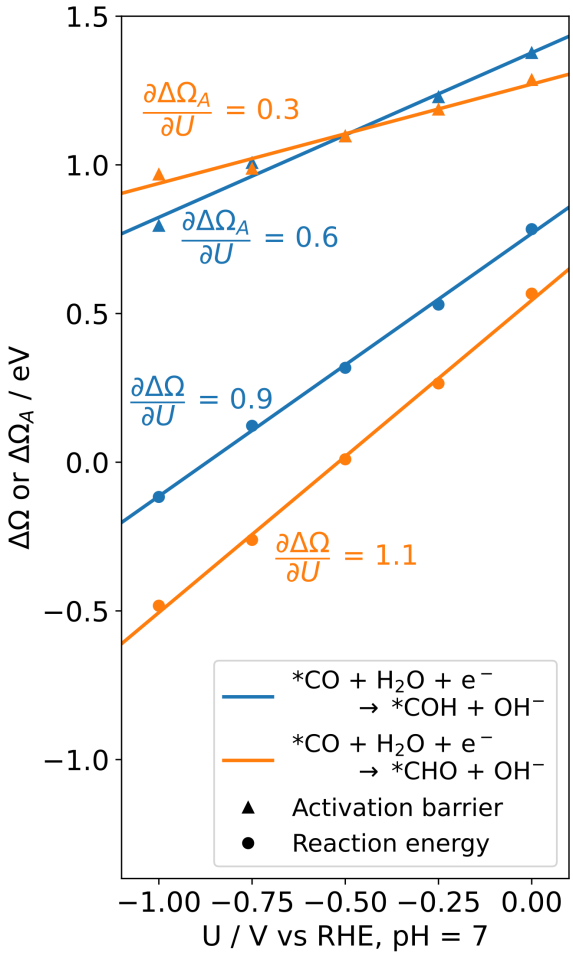

Figure 2: Constant potential reaction energetics of alkaline CO protonation on Cu (100) at pH = 7. Circles illustrate the potential dependent overall reaction energy, while triangles show the potential dependent activation barriers.

Competition between the formation of ∗CHO and ∗COH in the CO2RR has been investigated in numerous previous studies, with consideration given to both thermodynamics[9,34,40,47–49] and kinetics.[11–13,16] For thermodynamics, where the distinction between alkaline and acidic pathway vanishes, the formation of ∗CHO is favored over formation of ∗COH by a significant margin on Cu (100) and Cu (111). Activation barriers, when computed (via the acidic pathway), have previously found the ∗COH pathway to be favored.[11–13,16] A recent

study[50] investigated trends in the electrochemical barrier among ∗C, ∗N, and ∗O adsorbates, and found that protonation of carbon to be hardest, and protonation of oxygen to be easiest, in support of the ∗COH pathway being favored kinetically. Notably, most of these activation barriers were calculated considering only the acidic pathway, which we have demonstrated is likely not as physically relevant for the CO2RR. In support of previous investigations that considered the acidic pathway, our investigation into the alkaline pathway indicates that while the formation of ∗CHO is favored thermodynamically, formation of ∗COH has a lower activation barrier under highly reducing conditions, while ∗CHO formation is favored at low overpotential.

We also investigated the possibility of isomerization between ∗CHO and ∗COH, discussed in SI Note 6. While none of the pathways we investigated resulted in an activation barrier much lower than 1.5 eV (i.e., higher than the calculated barriers to direct formation of ∗CHO at negative bias), it is difficult to prove the non-existence of a feasible reaction coordinate. As we discuss in further detail below, an alternative possibility is the formation of ∗CHO via thermochemical hydrogenation with ∗H, which we find to have a barrier of about 0.75 eV. Our results suggest, but do not rigorously prove, that isomerization between ∗CHO and ∗COH would not happen at an significant rate at room temperature.

We now turn our attention to the formation of the first carbon-carbon (C-C) bond in the CO2RR on Cu (100). We consider four separate pathways to this critical step in the CO2RR, written in Eqs 1-4,

$$*CO + *CO \rightarrow *OCCO \tag{6}$$

$$*CO + *C \rightarrow *CCO \tag{7}$$

$$*CO + *CHO \rightarrow *OCCHO \tag{8}$$

$$*CO + *COH \rightarrow *OCCOH \quad . \tag{9}$$

Given the high energetic barriers towards formation of ∗CHO, ∗COH, and by proxy ∗C

(since it is formed via the ∗COH pathway), we hypothesize that the surface coverage of these intermediates will be significantly lower than the coverage of ∗CO and so we neglect pathways that do not include ∗CO as a reactant. In the case of C-C bond formation, activation barriers were computed using the machine learning nudged elastic band (ML-NEB)[51] transition state search methodology. Potential control was achieved using the previously published mapping of constant charge to constant potential simulations, described in brief in SI Note 5 and in more detail in Ref. 36. As before, solvation was handled using implicit solvation as implemented in VASPsol.[38,39] The results of these calculations are illustrated in Figure 3.

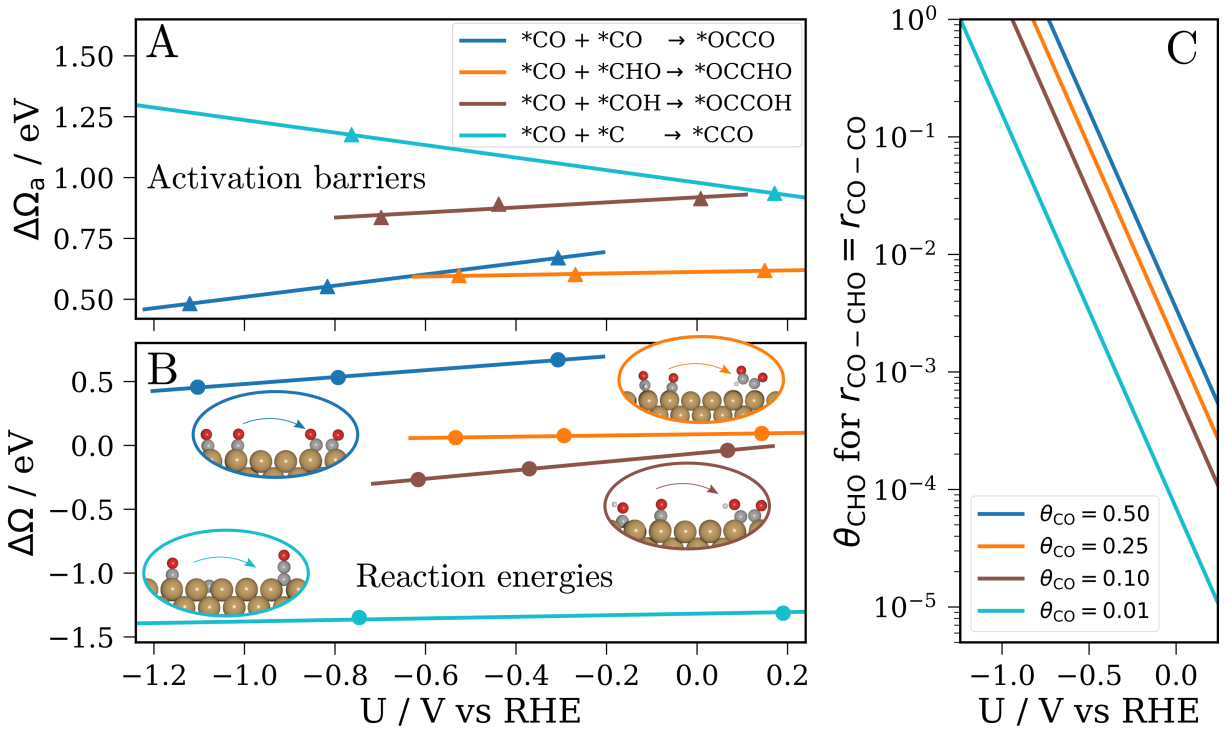

Figure 3: Constant potential reaction energetics for forming the first C-C bond in CO2RR on Cu (100) at pH = 7. Computed potential dependent activation barriers are shown in panel (A), while reaction energies are shown in panel (B). Panel (C) shows the steady state ∗CHO coverage, θ_{CHO}, needed for the rate of formation of ∗OCCHO to equal the rate of formation of ∗OCCO as a function of potential and steady state CO coverage, θ_{CO}.

Interestingly, although CO dimerization (Eq. 6) has the highest reaction energy at all potentials, the barrier is the lowest at high overpotentials, and competitive with ∗CO+∗CHO coupling (Eq. 8) at low overpotentials, in qualitative agreement with a recent study by

Hirunsit and coworkers.[52] In fact, the data presented in Figure 3 suggest that the Brønsted-Evans-Polyani (BEP) scaling would have a negative slope for these reactions, in contrast to most cases. The results illustrated in panels (a) and (b) of Figure 3 highlight an important consideration when using thermodynamic data for mechanistic discovery. BEP scaling is a very powerful tool that has led to fundamental insights and improvements in catalyst design, and results from electronic coupling of the adsorbate with the metal.[53,54] For a given reaction, e.g. H_2 dissociation, the correlation between the reaction energy and activation barrier will hold very well across transition metal surfaces, a result of the metal *d*-band being well characterized as just a rectangular density with filling defined by its center relative to the Fermi level. However, greater care must be taken when rather than varying the metal with a fixed chemistry, the chemistry is varied with a fixed metal as is the case in Figure 3. Varying the chemistry with a fixed metal can lead to a predictive BEP scaling with positive slope[55–57] when the chemistries being studied (in particular, the orbital interaction with metal) is similar across adsorbates, but it can also fail as we see here. With this in mind, care must be taken when relying solely on thermodynamic information to drive mechanistic discovery.

We note that, as has been discussed in previously,[36,37,58–61] the activation barriers presented in Figure 3 are dependent on the applied bias due to a change in the field-dipole interaction across the reaction coordinate. Furthermore, while microkinetic analysis has led to powerful insights for a variety of processes, it can be limited when applied to complicated and relatively flat potential energy surfaces such as in the CO2RR, as has been noted by Chan and coworkers.[32] For example, Ref. 62 illustrates that, given error estimates provided by the BEEF-vdW exchange correlation functional ensemble, predictions of CO2 hydrogenation selectivity vary between 0.2 and 0.8 at high temperature, limiting the usefulness of microkinetic analysis. For this reason, we deliberately chose not to perform microkinetic analysis on our model system.

Our results suggest that at high overpotentials, i.e. strongly reducing conditions, CO

dimerization (Eq. 6) is the dominant pathway to the formation of C-C bonds on Cu (100). At lower overpotentials, there is competition between CO dimerization and coupling of ∗CO+∗CHO (Eq. 8). Figure 3 (c) shows the steady state coverage of ∗CHO, θ_{CHO}, needed for the rate of Eq. 6 to be equal to the rate of Eq. 8 as a function of applied bias and the steady state ∗CO coverage, θ_{CO}. As seen in the figure, the coupling of ∗CO+∗CHO is unlikely to be competitive with CO dimerization even at low overpotentials unless θ_{CO} is very low. Two computational investigations that utilize a complete microkinetic model found θ_{CO} to be between 0.25 and 0.4 between 0 and -1 V vs RHE,[9,11] corresponding approximately to the orange line in Figure 3 (c). In this case, the needed θ_{CHO} at low overpotential ranges from 10^{-3} to 10^{-1}. While these coverages are likely higher than is achieved in reality (the previously published microkinetic models[11] estimate θ_{CHO} to be on the order of 10^{-12}), it cannot be rigorously ruled out without a complete alkaline pathway microkinetic model. Our finding is in qualitative disagreement with a previously published study,[35] which found the coupling of ∗CO and ∗CHO to be the dominant pathway at high overpotentials. We hypothesize this difference is due to both the correction to the reaction energy of the alkaline pathway (SI Note 4) and the finite cell height correction (described in SI Note 7 and in Ref. 36), the latter of which was not known at the time of the publication of the previous study. The finite cell height effect can lead to very large corrections, especially for constant potential CPET reactions such as those found in CO protonation (see SI Note 7).

Our results support experimental findings on polycrystalline copper at neutral pH,[63,64] summarized in Table 1. At low overpotential ($U > -0.7$ V vs RHE), activity on Cu is dominated by the hydrogen evolution reaction, since the current is low enough that transport of alternative proton donors (hydronium cations, bicarbonate) is not limiting. At moderate to high overpotential ($-0.7 > U > -1.1$ V vs RHE), HER activity is decreased, and activity to C_{2+} products reaches a maximum at around –1 V vs RHE. In this regime, activity is driven by a combination of protonation from water and transport of proton donors with lower pKa, and possibly surface hydrogenation pathways. We computed the activation barrier to hydro-

genate ∗CO to form ∗CHO via a surface bound ∗H to be around 0.75 eV, substantially lower than the activation barrier to protonate from water at –1 V vs RHE (see SI Note 9 for more details). At very high overpotentials, ($U < -1.1$ V vs RHE) the applied bias is so high that protonation from water is more accessible, and so HER and formation of highly protonated products such as methane begin to increase again. At these potentials, accumulation of hydroxide driven by poor transport also leads to a decrease in the local CO_2 concentration due to equilibrium with carbonate anions, further reducing the rate of the CO2RR. In the context of the relative selectivity to C_1 and C_{2+} products, our findings illustrate that transport is a critical component in catalyst performance that is often overlooked in computational investigations.[65]

Table 1: Summarized experimental observations[63,64] of primary products during electroreduction of CO_2 on polycrystalline copper.

Applied Bias / V vs RHE	Experimental result[63,64]	Predicted results (this work)
above -0.7	HER dominates	Acidic HER dominates (low exchange current means proton transport not limiting)
-0.7 to -1.1	HER decreases significantly, ethylene production begins to increase.	Local pH near interface increases, inhibiting acidic HER. CO dimerization occurs as θ_{CO} increases.
below -1.1	C-C bond formation reduces, methane and hydrogen production increases.	Alkaline HER enabled by high overpotential resulting in increased θ_H and possible thermochemical hydrogenation of CO.

As a final consideration, we investigated the role of dispersion effects in the key reaction pathways computed here. It is clear that dispersion is important in accurately describing water-water interactions,[66,67] but the role of dispersion forces in describing CPET reactions at metal surfaces, to our knowledge, has not been investigated. DFT at the semi-local level, in particular functionals such as PBE[68] and RPBE,[69] are the primary workhorse for computational catalysis studies.[70] While RPBE performs very well for chemisorption of molecules on metal surfaces, typically outperforming meta-GGA and hybrid functionals,

it shows poorer performance for systems where dispersion forces are significant.[71–75] We compared RPBE with RPBE+D3 with the damping of Grimme,[76] which offers a low-cost approach for incorporating dispersion, and can be found in SI Note 8. As we discuss below, since we include only a very limited explicit solvent representation and dispersion is an isotropic attractive force, our estimate may be different than for the fully molecular system.

To investigate the effect of dispersion more rigorously, we considered the B97M–rV exchange correlation functional, a meta-GGA which directly incorporates long-range van der Waals interactions,[77,78] keeping in mind that moving up Jacob's ladder is by no means a guarantee for improved performance in describing e.g. chemisorption.[74] Due to the high computational cost in using meta-GGA functionals on systems in our work, we performed single-point calculations on the converged RPBE geometries. The results of our calculations are illustrated in Figure 4.

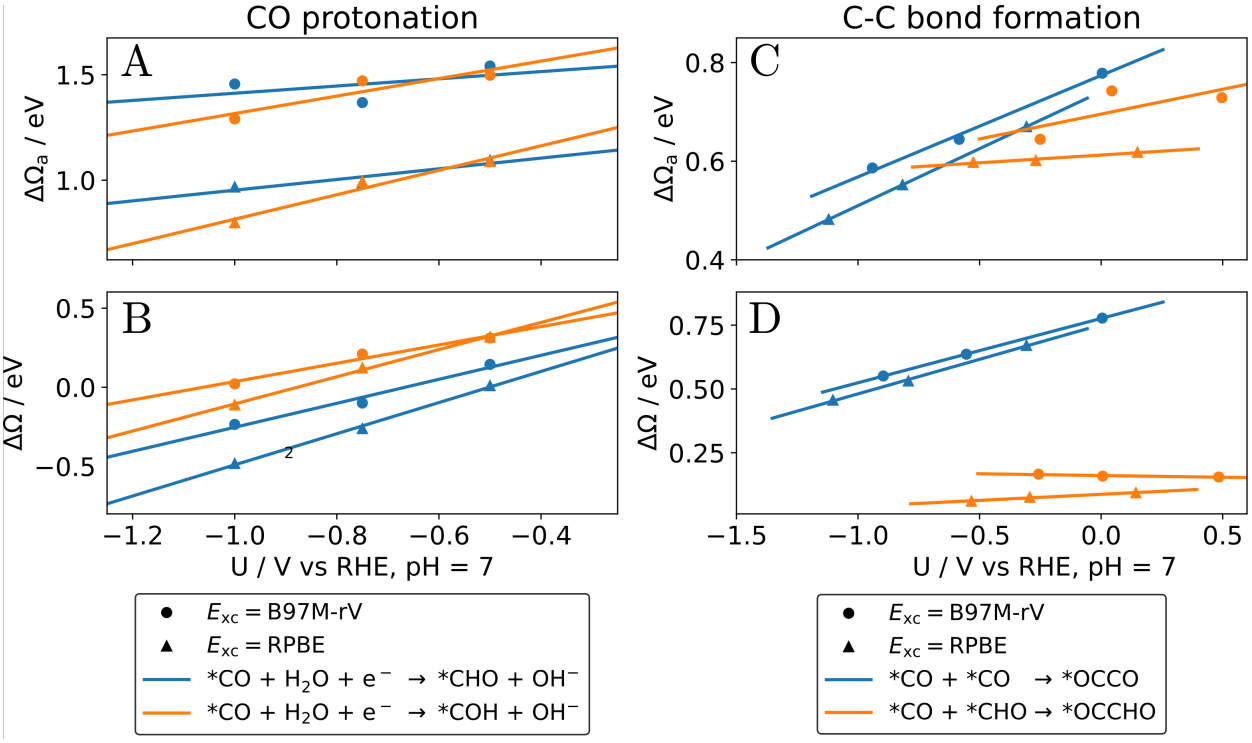

Figure 4: Comparison of the GGA-DFT functional RPBE with the meta-GGA functional B97M-rV for reaction energies and activation barriers relevant to the CO2RR on Cu (100). Panels (a) and (b) show the activation barrier and reaction energies, respectively, for CO protonation to form ∗CHO and ∗COH. Panels (c) and (d) show the activation barrier and reaction energies, respectively, for C-C bond formation as described in Equations 6 and 8. B97M–rV data illustrate single-point calculations on converged RPBE geometries due to the high computational cost and large simulation cell sizes used.

We find that all qualitative trends remain unchanged when the meta-GGA functional is used. When describing alkaline CO protonation to form ∗CHO and ∗COH, shown in panels Figure 4 (A) and (B), B97M–rV predicts ∗CHO to be favored thermodynamically across all tested potentials, while formation of ∗COH is favored kinetically at high overpotential. In describing C-C bond formation, shown in Figure 4 panels (C) and (D), B97M–rV predicts very similar trends of activation barriers and reaction energies for both CO dimerization and coupling of ∗CO+∗CHO.

Given the similarities in qualitative trends between the two functionals, we find that inclusion of dispersion interactions and non-local effects in the B97M–rV functional are likely not critically important for either alkaline CO protonation or C–C bond formation. However, we note that the effect of dispersion depends strongly on the number of explicit water molecules included in the system. As we chose to use a minimal representation of explicit electrolyte and instead rely on implicit solvation, the role of dispersion may change in CPET reactions.

In summary, we have presented a theoretical and computational investigation into the pathways for formation of C_{2+} products under alkaline conditions in the electrochemical CO_2 reduction reaction. Based on a comparison of computed reaction energies and activation energies for the Volmer reaction on Cu (100) and published experimental results, we find that the alkaline pathway is more physically relevant for the CO2RR, even when the bulk pH is acidic and particularly when it is neutral or alkaline. We suggest modeling the final state of hydroxide via the computational hydrogen electrode, as hydroxide near the surface is not an adequate model for fully solvated hydroxide. Given our calculated alkaline activation energies for CO protonation, we find that ∗COH formation is the preferred pathway at overpotentials relevant for formation of C_{2+} products, even though ∗COH formation is more thermodynamically unfavorable. We find a reasonably low activation barrier (0.75 eV) for the thermochemical hydrogenation of CO, i.e. ∗H+∗CO→ ∗CHO, suggesting that resolving the role of similar non electrochemical steps could be an interesting target of future

work. Our investigation into the formation of the first carbon-carbon bond in the CO2RR suggest that thermodynamics alone can be misleading for mechanism identification; the most thermodynamically favorable step (Eq. 7) was found to be the least favorable kinetically. Instead the most endergonic pathway (CO dimerization) was found to have the lowest activation barrier at strongly reducing conditions. At lower overpotentials, the coupling of $*$CO and $*$CHO has a lower activation barrier, but it is likely that the steady-state coverage of $*$CHO is too low for this pathway to be dominant on Cu (100). By comparison to the meta-GGA functional B97M–rV, which includes long-range dispersion interactions, we find that inclusion of dispersion and non-local effects largely do not lead to qualitatively different findings, which suggests that these effects are not critical to describing the chemistries involved in the CO2RR. Our computational model could be significantly improved. Particularly for alkaline pathways, identification of a transition state is complicated by poor description of the final state. Future investigations with a fully molecular model, for example with enhanced sampling techniques that are grand canonical not only in electrons, but also in electrolyte ions, would significantly improve confidence in the conclusions presented here.

Acknowledgement

We thank the U.S. Department of Energy, Office of Science, Office of Advanced Scientific Computing Research, Scientific Discovery through Advanced Computing (SciDAC) program for support. This research used resources of the National Energy Research Scientific Computing Center, a DOE Office of Science User Facility supported by the Office of Science of the U.S. Department of Energy under Contract No. DE-AC02-05CH11231. This research also used computing resources at the Molecular Graphics and Computation Facility operated by the College of Chemistry at the University of California, Berkeley, grant No. NIH S10OD023532

Supporting Information

Supporting information for this work, including figures and tables referenced in the text, as well as tables of all data required to reproduce the figures in this work, are available. This material is available free of charge via the Internet at http://pubs.acs.org.

References

(1) Stocker, T. et al. In *Climate Change 2013: The Physical Science Basis. Contribution of Working Group I to the Fifth Assessment Report of the Intergovernmental Panel on Climate Change*; Stocker, T., Qin, D., Plattner, G.-K., Tignor, M., Allen, S., Boschung, J., Nauels, A., Xia, Y., Bex, V., Midgley, P., Eds.; Cambridge University Press: Cambridge, United Kingdom and New York, NY, USA, 2013; Chapter TS, p 33–115.

(2) Nitopi, S.; Bertheussen, E.; Scott, S. B.; Liu, X.; Engstfeld, A. K.; Horch, S.; Seger, B.; Stephens, I. E. L.; Chan, K.; Hahn, C.; Nørskov, J. K.; Jaramillo, T. F.; Chorkendorff, I. Progress and Perspectives of Electrochemical CO2 Reduction on Copper in Aqueous Electrolyte. *Chemical Reviews* **2019**, *119*, 7610–7672.

(3) De Luna, P.; Hahn, C.; Higgins, D.; Jaffer, S. A.; Jaramillo, T. F.; Sargent, E. H. What would it take for renewably powered electrosynthesis to displace petrochemical processes? *Science* **2019**, *364*, eaav3506.

(4) Velasco-Velez, J.-J.; Wu, C. H.; Pascal, T. A.; Wan, L. F.; Guo, J.; Prendergast, D.; Salmeron, M. The structure of interfacial water on gold electrodes studied by x-ray absorption spectroscopy. *Science* **2014**, *346*, 831–834.

(5) Medford, A. J.; Vojvodic, A.; Hummelshøj, J. S.; Voss, J.; Abild-Pedersen, F.; Studt, F.; Bligaard, T.; Nilsson, A.; Nørskov, J. K. From the Sabatier principle to a predictive theory of transition-metal heterogeneous catalysis. *Journal of Catalysis* **2015**, *328*, 36–42.

(6) Björketun, M. E.; Zeng, Z.; Ahmed, R.; Tripkovic, V.; Thygesen, K. S.; Rossmeisl, J. Avoiding pitfalls in the modeling of electrochemical interfaces. *Chemical Physics Letters* **2013**, *555*, 145–148.

(7) Gauthier, J. A.; Chen, L. D.; Bajdich, M.; Chan, K. Implications of the fractional charge of hydroxide at the electrochemical interface. *Physical Chemistry Chemical Physics* **2020**, *22*, 6964–6969.

(8) Todorova, T. K.; Schreiber, M. W.; Fontecave, M. Mechanistic understanding of CO2 reduction reaction (CO2RR) toward multicarbon products by heterogeneous copper-based catalysts. *ACS Catalysis* **2019**, *10*, 1754–1768.

(9) Liu, X.; Xiao, J.; Peng, H.; Hong, X.; Chan, K.; Nørskov, J. K. Understanding trends in electrochemical carbon dioxide reduction rates. *Nature Communications* **2017**, *8*, 15438.

(10) Liu, F.; Kulik, H. J. Impact of approximate DFT density delocalization error on potential energy surfaces in transition metal chemistry. *Journal of Chemical Theory and Computation* **2019**, *16*, 264–277.

(11) Peng, H.; Tang, M. T.; Liu, X.; Lamoureux, P. S.; Bajdich, M.; Abild-Pedersen, F. The role of atomic carbon in directing electrochemical CO (2) reduction to multicarbon products. *Energy & Environmental Science* **2021**, *14*, 473–482.

(12) Zhao, Q.; Carter, E. A. Revisiting competing paths in electrochemical CO2 reduction on copper via embedded correlated wavefunction theory. *Journal of Chemical Theory and Computation* **2020**, *16*, 6528–6538.

(13) Zhao, Q.; Martirez, J. M. P.; Carter, E. A. Revisiting Understanding of Electrochemical CO2 Reduction on Cu (111): Competing Proton-Coupled Electron Transfer Reaction Mechanisms Revealed by Embedded Correlated Wavefunction Theory. *Journal of the American Chemical Society* **2021**, *143*, 6152–6164.

(14) Nie, X.; Esopi, M. R.; Janik, M. J.; Asthagiri, A. Selectivity of CO2 reduction on copper electrodes: the role of the kinetics of elementary steps. *Angewandte Chemie International Edition* **2013**, *52*, 2459–2462.

(15) Hirunsit, P. Electroreduction of carbon dioxide to methane on copper, copper–silver, and copper–gold catalysts: a DFT study. *The Journal of Physical Chemistry C* **2013**, *117*, 8262–8268.

(16) Hussain, J.; Jonsson, H.; Skúlason, E. Calculations of product selectivity in electrochemical CO2 reduction. *ACS Catalysis* **2018**, *8*, 5240–5249.

(17) Huang, J. E.; Li, F.; Ozden, A.; Rasouli, A. S.; de Arquer, F. P. G.; Liu, S.; Zhang, S.; Luo, M.; Wang, X.; Lum, Y., et al. CO2 electrolysis to multicarbon products in strong acid. *Science* **2021**, *372*, 1074–1078.

(18) Monteiro, M. C.; Liu, X.; Hagedoorn, B. J.; Snabilié, D. D.; Koper, M. T. Interfacial pH Measurements Using a Rotating Ring-Disc Electrode with a Voltammetric pH Sensor. *ChemElectroChem* **2022**, *9*, e202101223.

(19) Monteiro, M. C.; Mirabal, A.; Jacobse, L.; Doblhoff-Dier, K.; Barton, S. C.; Koper, M. T. Time-Resolved Local pH Measurements during CO2 Reduction Using Scanning Electrochemical Microscopy: Buffering and Tip Effects. *JACS Au* **2021**, *1*, 1915–1924.

(20) Gupta, N.; Gattrell, M.; MacDougall, B. Calculation for the cathode surface concentrations in the electrochemical reduction of CO 2 in KHCO 3 solutions. *Journal of Applied Electrochemistry* **2006**, *36*, 161–172.

(21) Lu, X.; Zhu, C.; Wu, Z.; Xuan, J.; Francisco, J. S.; Wang, H. In situ observation of the pH gradient near the gas diffusion electrode of CO2 reduction in alkaline electrolyte. *Journal of the American Chemical Society* **2020**, *142*, 15438–15444.

(22) Welch, A. J.; DuChene, J. S.; Tagliabue, G.; Davoyan, A.; Cheng, W.-H.; Atwater, H. A. Nanoporous gold as a highly selective and active carbon dioxide reduction catalyst. *ACS Applied Energy Materials* **2018**, *2*, 164–170.

(23) Welch, A. J.; Fenwick, A. Q.; Böhme, A.; Chen, H.-Y.; Sullivan, I.; Li, X.; DuChene, J. S.; Xiang, C.; Atwater, H. A. Operando local pH measurement within gas diffusion electrodes performing electrochemical carbon dioxide reduction. *The Journal of Physical Chemistry C* **2021**, *125*, 20896–20904.

(24) Bui, J. C.; Kim, C.; Weber, A. Z.; Bell, A. T. Dynamic Boundary Layer Simulation of Pulsed CO2 Electrolysis on a Copper Catalyst. *ACS Energy Letters* **2021**, *6*, 1181–1188.

(25) Hashiba, H.; Weng, L.-C.; Chen, Y.; Sato, H. K.; Yotsuhashi, S.; Xiang, C.; Weber, A. Z. Effects of electrolyte buffer capacity on surface reactant species and the reaction rate of CO2 in Electrochemical CO2 reduction. *The Journal of Physical Chemistry C* **2018**, *122*, 3719–3726.

(26) Dunwell, M.; Yang, X.; Setzler, B. P.; Anibal, J.; Yan, Y.; Xu, B. Examination of near-electrode concentration gradients and kinetic impacts on the electrochemical reduction of CO2 using surface-enhanced infrared spectroscopy. *ACS Catalysis* **2018**, *8*, 3999–4008.

(27) Monteiro, M. C.; Jacobse, L.; Touzalin, T.; Koper, M. T. Mediator-free SECM for probing the diffusion layer pH with functionalized gold ultramicroelectrodes. *Analytical Chemistry* **2019**, *92*, 2237–2243.

(28) Bagotzky, V.; Osetrova, N. Investigations of hydrogen ionization on platinum with the help of micro-electrodes. *Journal of Electroanalytical Chemistry and Interfacial Electrochemistry* **1973**, *43*, 233–249.

(29) Marković, N.; Grgur, B.; Ross, P. N. Temperature-dependent hydrogen electrochemistry on platinum low-index single-crystal surfaces in acid solutions. *The Journal of Physical Chemistry B* **1997**, *101*, 5405–5413.

(30) Strmcnik, D.; Uchimura, M.; Wang, C.; Subbaraman, R.; Danilovic, N.; Van Der Vliet, D.; Paulikas, A. P.; Stamenkovic, V. R.; Markovic, N. M. Improving the hydrogen oxidation reaction rate by promotion of hydroxyl adsorption. *Nature Chemistry* **2013**, *5*, 300.

(31) Lamoureux, P. S.; Singh, A. R.; Chan, K. pH effects on hydrogen evolution and oxidation over Pt (111): insights from first-principles. *ACS Catalysis* **2019**, *9*, 6194–6201.

(32) Govindarajan, N.; Kastlunger, G.; Heenen, H. H.; Chan, K. Improving the intrinsic activity of electrocatalysts for sustainable energy conversion: where are we and where can we go? *Chemical Science* **2022**, *13*, 14–26.

(33) Sun, Z.; Hu, Y.; Zhou, D.; Sun, M.; Wang, S.; Chen, W. Factors Influencing the Performance of Copper-Bearing Catalysts in the CO2 Reduction System. *ACS Energy Letters* **2021**, *6*, 3992–4022.

(34) Kastlunger, G.; Wang, L.; Govindarajan, N.; Heenen, H. H.; Ringe, S.; Jaramillo, T.; Hahn, C.; Chan, K. Using pH dependence for understanding mechanisms in electrochemical CO reduction. *ChemRxiv* **2021**,

(35) Goodpaster, J. D.; Bell, A. T.; Head-Gordon, M. Identification of possible pathways for C–C bond formation during electrochemical reduction of CO2: New theoretical insights from an improved electrochemical model. *The Journal of Physical Chemistry Letters* **2016**, *7*, 1471–1477.

(36) Gauthier, J. A.; Dickens, C. F.; Ringe, S.; Chan, K. Practical considerations for continuum models applied to surface electrochemistry. *ChemPhysChem* **2019**, *20*, 3074–3080.

(37) Gauthier, J. A.; Dickens, C. F.; Heenen, H. H.; Vijay, S.; Ringe, S.; Chan, K. Unified approach to implicit and explicit solvent simulations of electrochemical reaction energetics. *Journal of Chemical Theory and Computation* **2019**, *15*, 6895–6906.

(38) Mathew, K.; Sundararaman, R.; Letchworth-Weaver, K.; Arias, T.; Hennig, R. G. Implicit solvation model for density-functional study of nanocrystal surfaces and reaction pathways. *The Journal of Chemical Physics* **2014**, *140*, 084106.

(39) Mathew, K.; Kolluru, V. C.; Mula, S.; Steinmann, S. N.; Hennig, R. G. Implicit self-consistent electrolyte model in plane-wave density-functional theory. *The Journal of Chemical Physics* **2019**, *151*, 234101.

(40) Liu, X.; Schlexer, P.; Xiao, J.; Ji, Y.; Wang, L.; Sandberg, R. B.; Tang, M.; Brown, K. S.; Peng, H.; Ringe, S.; Hahn, C.; Jaramillo, T. F.; Nørskov, J. K.; Chan, K. pH effects on the electrochemical reduction of CO (2) towards C 2 products on stepped copper. *Nature Communications* **2019**, *10*, 32.

(41) Tang, M. T.; Liu, X.; Ji, Y.; Norskov, J. K.; Chan, K. Modeling Hydrogen Evolution Reaction Kinetics through Explicit Water–Metal Interfaces. *The Journal of Physical Chemistry C* **2020**, *124*, 28083–28092.

(42) Nørskov, J. K.; Rossmeisl, J.; Logadottir, A.; Lindqvist, L.; Kitchin, J. R.; Bligaard, T.; Jonsson, H. Origin of the overpotential for oxygen reduction at a fuel-cell cathode. *The Journal of Physical Chemistry B* **2004**, *108*, 17886–17892.

(43) Chen, L. D.; Bajdich, M.; Martirez, J. M. P.; Krauter, C. M.; Gauthier, J. A.; Carter, E. A.; Luntz, A. C.; Chan, K.; Nørskov, J. K. Understanding the apparent fractional charge of protons in the aqueous electrochemical double layer. *Nature Communications* **2018**, *9*, 3202.

(44) Henkelman, G.; Jónsson, H. A dimer method for finding saddle points on high dimen-

sional potential surfaces using only first derivatives. *The Journal of Chemical Physics* **1999**, *111*, 7010–7022.

(45) Henkelman, G.; Uberuaga, B. P.; Jónsson, H. A climbing image nudged elastic band method for finding saddle points and minimum energy paths. *The Journal of Chemical Physics* **2000**, *113*, 9901–9904.

(46) Henkelman, G.; Jónsson, H. Improved tangent estimate in the nudged elastic band method for finding minimum energy paths and saddle points. *The Journal of Chemical Physics* **2000**, *113*, 9978–9985.

(47) Hussain, J.; Skúlason, E.; Jónsson, H. Computational study of electrochemical CO2 reduction at transition metal electrodes. *Procedia Computer Science* **2015**, *51*, 1865–1871.

(48) Peterson, A. A.; Nørskov, J. K. Activity descriptors for CO2 electroreduction to methane on transition-metal catalysts. *The Journal of Physical Chemistry Letters* **2012**, *3*, 251–258.

(49) Shi, C.; Hansen, H. A.; Lausche, A. C.; Nørskov, J. K. Trends in electrochemical CO 2 reduction activity for open and close-packed metal surfaces. *Physical Chemistry Chemical Physics* **2014**, *16*, 4720–4727.

(50) Patel, A. M.; Vijay, S.; Kastlunger, G.; Nørskov, J. K.; Chan, K. Generalizable Trends in Electrochemical Protonation Barriers. *The Journal of Physical Chemistry Letters* **2021**, *12*, 5193–5200.

(51) Torres, J. A. G.; Jennings, P. C.; Hansen, M. H.; Boes, J. R.; Bligaard, T. Low-scaling algorithm for nudged elastic band calculations using a surrogate machine learning model. *Physical Review Letters* **2019**, *122*, 156001.

(52) Santatiwongchai, J.; Faungnawakij, K.; Hirunsit, P. Comprehensive Mechanism of CO2 Electroreduction toward Ethylene and Ethanol: The Solvent Effect from Explicit Water–Cu (100) Interface Models. *ACS Catalysis* **2021**, *11*, 9688–9701.

(53) Hammer, B.; Norskov, J. Why gold is the noblest of all the metals. *Nature* **1995**, *376*, 238.

(54) Pallassana, V.; Neurock, M. Electronic factors governing ethylene hydrogenation and dehydrogenation activity of pseudomorphic PdML/Re (0001), PdML/Ru (0001), Pd (111), and PdML/Au (111) surfaces. *Journal of Catalysis* **2000**, *191*, 301–317.

(55) Singh, A. R.; Rohr, B. A.; Gauthier, J. A.; Nørskov, J. K. Predicting chemical reaction barriers with a machine learning model. *Catalysis Letters* **2019**, *149*, 2347–2354.

(56) Wang, S. et al. Universal transition state scaling relations for (de) hydrogenation over transition metals. *Physical Chemistry Chemical Physics* **2011**, *13*, 20760–20765.

(57) Wang, S.; Temel, B.; Shen, J.; Jones, G.; Grabow, L. C.; Studt, F.; Bligaard, T.; Abild-Pedersen, F.; Christensen, C. H.; Nørskov, J. K. Universal Brønsted-Evans-Polanyi relations for C–C, C–O, C–N, N–O, N–N, and O–O dissociation reactions. *Catalysis Letters* **2011**, *141*, 370–373.

(58) Montoya, J. H.; Shi, C.; Chan, K.; Nørskov, J. K. Theoretical insights into a CO dimerization mechanism in CO2 electroreduction. *The Journal of Physical Chemistry Letters* **2015**, *6*, 2032–2037.

(59) Gauthier, J. A.; Ringe, S.; Dickens, C. F.; Garza, A. J.; Bell, A. T.; Head-Gordon, M.; Nørskov, J. K.; Chan, K. Challenges in Modeling Electrochemical Reaction Energetics with Polarizable Continuum Models. *ACS Catalysis* **2018**, *9*, 920–931.

(60) Vijay, S.; Gauthier, J. A.; Heenen, H. H.; Bukas, V. J.; Kristoffersen, H. H.; Chan, K.

Dipole-Field Interactions Determine the CO2 Reduction Activity of 2D Fe–N–C Single-Atom Catalysts. *ACS Catalysis* **2020**, *10*, 7826–7835.

(61) Chan, K. A few basic concepts in electrochemical carbon dioxide reduction. *Nature Communications* **2020**, *11*, 1–4.

(62) Yang, N.; Medford, A. J.; Liu, X.; Studt, F.; Bligaard, T.; Bent, S. F.; Nørskov, J. K. Intrinsic selectivity and structure sensitivity of rhodium catalysts for C2+ oxygenate production. *Journal of the American Chemical Society* **2016**, *138*, 3705–3714.

(63) Hori, Y.; Murata, A.; Takahashi, R. Formation of hydrocarbons in the electrochemical reduction of carbon dioxide at a copper electrode in aqueous solution. *Journal of the Chemical Society, Faraday Transactions 1: Physical Chemistry in Condensed Phases* **1989**, *85*, 2309–2326.

(64) Kuhl, K. P.; Cave, E. R.; Abram, D. N.; Jaramillo, T. F. New insights into the electrochemical reduction of carbon dioxide on metallic copper surfaces. *Energy & Environmental Science* **2012**, *5*, 7050–7059.

(65) Singh, M. R.; Goodpaster, J. D.; Weber, A. Z.; Head-Gordon, M.; Bell, A. T. Mechanistic insights into electrochemical reduction of CO2 over Ag using density functional theory and transport models. *Proceedings of the National Academy of Sciences* **2017**, *114*, E8812–E8821.

(66) Klimeš, J.; Michaelides, A. Perspective: Advances and challenges in treating van der Waals dispersion forces in density functional theory. *The Journal of Chemical Physics* **2012**, *137*, 120901.

(67) Bjorneholm, O.; Hansen, M. H.; Hodgson, A.; Liu, L.-M.; Limmer, D. T.; Michaelides, A.; Pedevilla, P.; Rossmeisl, J.; Shen, H.; Tocci, G., et al. Water at interfaces. *Chemical Reviews* **2016**, *116*, 7698–7726.

(68) Perdew, J. P.; Burke, K.; Ernzerhof, M. Generalized gradient approximation made simple. *Physical Review Letters* **1996**, *77*, 3865.

(69) Hammer, B.; Hansen, L. B.; Nørskov, J. K. Improved adsorption energetics within density-functional theory using revised Perdew-Burke-Ernzerhof functionals. *Physical Review B* **1999**, *59*, 7413.

(70) Haunschild, R.; Barth, A.; Marx, W. Evolution of DFT studies in view of a scientometric perspective. *Journal of Cheminformatics* **2016**, *8*, 1–12.

(71) Wellendorff, J.; Lundgaard, K. T.; Møgelhøj, A.; Petzold, V.; Landis, D. D.; Nørskov, J. K.; Bligaard, T.; Jacobsen, K. W. Density functionals for surface science: Exchange-correlation model development with Bayesian error estimation. *Physical Review B* **2012**, *85*, 235149.

(72) Wellendorff, J.; Silbaugh, T. L.; Garcia-Pintos, D.; Nørskov, J. K.; Bligaard, T.; Studt, F.; Campbell, C. T. A Benchmark Database for Adsorption Bond Energies to Transition Metal Surfaces and Comparison to Selected DFT Functionals. *Surface Science* **2015**, *640*, 36–44.

(73) Lundgaard, K. T.; Wellendorff, J.; Voss, J.; Jacobsen, K. W.; Bligaard, T. mBEEF-vdW: Robust fitting of error estimation density functionals. *Physical Review B* **2016**, *93*, 235162.

(74) Sharada, S. M.; Karlsson, R. K.; Maimaiti, Y.; Voss, J.; Bligaard, T. Adsorption on transition metal surfaces: Transferability and accuracy of DFT using the ADS41 dataset. *Physical Review B* **2019**, *100*, 035439.

(75) Lininger, C. N.; Gauthier, J. A.; Li, W.-L.; Rossomme, E.; Welborn, V. V.; Lin, Z.; Head-Gordon, T.; Head-Gordon, M.; Bell, A. T. Challenges for density functional theory: calculation of CO adsorption on electrocatalytically relevant metals. *Physical Chemistry Chemical Physics* **2021**, *23*, 9394–9406.

(76) Grimme, S.; Antony, J.; Ehrlich, S.; Krieg, H. A consistent and accurate ab initio parametrization of density functional dispersion correction (DFT-D) for the 94 elements H-Pu. *The Journal of Chemical Physics* **2010**, *132*, 154104.

(77) Mardirossian, N.; Head-Gordon, M. Mapping the genome of meta-generalized gradient approximation density functionals: The search for B97M-V. *The Journal of Chemical Physics* **2015**, *142*, 074111.

(78) Mardirossian, N.; Ruiz Pestana, L.; Womack, J. C.; Skylaris, C.-K.; Head-Gordon, T.; Head-Gordon, M. Use of the rVV10 nonlocal correlation functional in the B97M-V density functional: Defining B97M-rV and related functionals. *The journal of Physical Chemistry Letters* **2017**, *8*, 35–40.

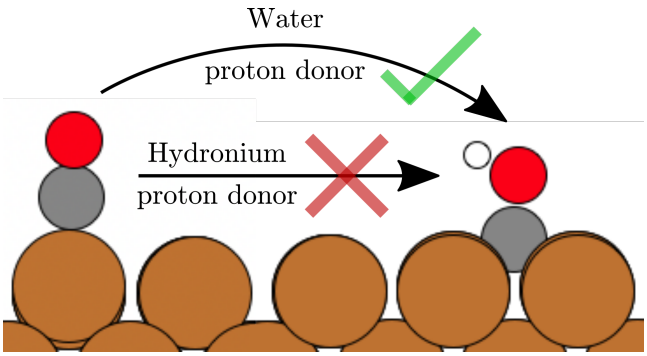
Water
proton donor
Hydronium
proton donor